CHEMISTRY OF MATERIALS

ARTICLE

pubs.acs.org/cm

Li_2FeSiO_4 Polymorphs Probed by ^6Li MAS NMR and ^{57}Fe Mössbauer Spectroscopy

Gregor Mali,[†,‡] Chutchamon Sirisopanaporn,[†,§,∥] Christian Masquelier,[§,∥] Darko Hanzel,[⊥] and Robert Dominko*[,†,∥]

[†]National Institute of Chemistry, POB 660, SI-1001 Ljubljana, Slovenia

[‡]EN-FIST Centre of Excellence, Dunajska 156, SI-1000 Ljubljana, Slovenia

[§]LRCS, Université de Picardie Jules Verne, 33 Rue Saint-Leu, 80039 Amiens, France

[∥]ALISTORE-ERI, 80039, 33 Rue Saint-Leu, Amiens Cedex, France

[⊥]Jozef Stefan Institute, Jamova 39, SI-1000 Ljubljana, Slovenia

Supporting Information

ABSTRACT: Several samples of pure Li_2FeSiO_4 polymorphs, prepared by hydrothermal synthesis and then quenched from either 400 °C ($Pmn2_1$), 700 °C ($P2_1/n$), or 900 °C ($Pmnb$), were thoroughly investigated by Mössbauer and NMR spectroscopy. ^{57}Fe Mössbauer spectroscopy showed that (i) iron in all the polymorphs existed in the divalent oxidation state, and (ii) chemical shifts and quadrupolar splittings correlated well with Fe−O bond lengths. ^6Li MAS NMR spectra of the three different polymorphs exhibit substantially different spinning-sideband patterns and slightly different isotropic shifts. The sideband patterns stemming from the anisotropic electron−nucleus dipole−dipole interaction reflect the arrangement of paramagnetic iron ions around lithium nuclei and allowed unambiguous assignments of ^6Li MAS NMR signals to crystallographically nonequivalent Li sites. Analysis of isotropic NMR shifts of ^6Li nuclei revealed that they comprised two contributions of comparable magnitude, a hyperfine (contact) shift and a pseudo-contact shift. Based on the structural models of Li_2FeSiO_4, both contributions could be successfully predicted by first-principles calculations. The contact shift was obtained from the hyperfine-coupling constant on ^6Li nuclei, which was calculated within a DFT/PAW approach, and the pseudo-contact shift was derived from the electron−nucleus dipolar matrix and the g-tensor, which was computed within the DFT/GIPAW frame.

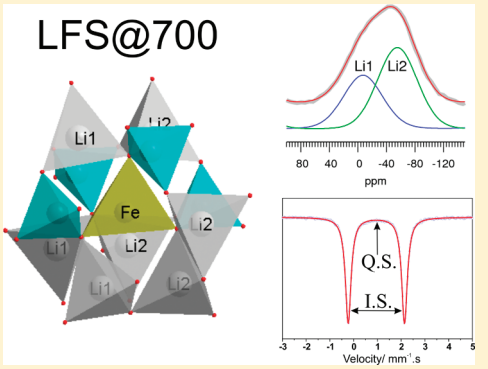

KEYWORDS: Mössbauer spectroscopy, MAS NMR, DFT/GIPAW, Li_2FeSiO_4, Li-ion batteries

INTRODUCTION

The interest in polyanionic materials as positive electrode materials for Li-ion batteries has increased dramatically after the first report on the electrochemical activity of $LiFePO_4$.[1] Oxygen atoms in the polyanionic framework structures are stabilized by X−O bonds (X = P, Si, B, ...) with a strong covalent nature. This makes polyanionic-based materials safer and more stable over prolonged cycling. An attractive member of this group is Li_2FeSiO_4 (LFS),[2,3] which is built on inexpensive and abundant raw materials. In recent works, small particles of LFS and proper electrode engineering have yielded electrodes with good cycling stability close to theoretical capacity.[4,5]

Besides addressing the challenge of enhancing the electrochemical performances of Li_2FeSiO_4 cathodes, the objective of our research is to attemtpt to understand the complex polymorphism of these silicates and correlate the structural informations obtained with the observed response upon Li^+ extraction/insertion. Global (crystal structures, extended, or localized defects) as well as local (Fe and Li environments, connectivity and orientations of AO_4 tetrahedra) structural parameters may indeed play a role for the thermodynamics and kinetics of Li^+ extraction from these structures.

Several polymorphs were recently isolated and characterized, based on careful X-ray diffraction (XRD) and neutron diffraction studies and transmission electron microscopy (TEM) investigation.[6−8] The proposed structural models for LFS were derived from Li_3PO_4 structures and can be roughly divided into two large subgroups: a low-temperature group[9] (denoted as β), and a high-temperature group[10] (denoted as γ). In both structural models, half of the tetrahedral sites, generated by a distorted hexagonal close packing of oxygen atoms, are occupied by cations, and the difference between polymorphs lies in the respective orientations of the filled tetrahedra and in their connectivity.

The above-described differences among the LFS polymorphs are generally observed in well-crystalline samples, while in

Received: November 7, 2010
Revised: March 19, 2011
Published: May 13, 2011

the samples prepared for the electrochemical characterization (with particles below 50 nm) or in the samples where a mixture of polymorphs is present, lower-quality XRD patterns may not enable a reliable determination of the structure. In such cases, the use of characterization techniques that can detect local environments of cations in the samples (for instance, NMR or Mössbauer spectroscopy) is of primary importance.

Meaningful parameters such as chemical shift (IS) and quadrupole splitting (QS) can be derived from Mössbauer spectra and provide information about iron coordination, valence state, and covalency of the iron−ligand bonds. It is generally accepted that, for a given oxidation state and for identical ligands, an increase in the covalency of the iron−ligands bonds corresponds to a decrease in the iron−ligands interatomic distances, which is translated to an observed decrease in the isomer shift.[11]

Nuclear magnetic resonance (NMR) spectroscopy has been used as a characterization technique for many lithium-containing materials for Li batteries.[12] Lithium NMR spectroscopy was particularly useful for the elucidation of structural motifs that did not exhibit long-range order and, thus, could not be analyzed by diffraction techniques.[13−15] Recently, MAS NMR spectroscopy of ^{6}Li nuclei has proved to be a very convenient tool that could distinguish between different Li_2MnSiO_4 polymorphs.[16] Lithium nuclei within polymorphs of Li_2MnSiO_4 or lithium nuclei occupying nonequivalent crystallographic lithium sites within a single polymorph exhibited NMR signals at different and well-resolved isotropic positions.

Several structural issues related to tetrahedral lithium-containing transition-metal silicates or phosphates have been studied by first-principles calculations.[17−20] For example, density-functional theory (DFT)-based calculations were able to predict the stability of pure Li_2MnSiO_4 polymorphs[17] and of $Li_2Fe_zMn_{1-z}SiO_4$ solid solutions.[20] In many cases, first-principles calculations also helped in the interpretation of NMR data—in particular, those related to the isotropic shifts detected in ^{6}Li or ^{7}Li NMR spectra.[21−23] Since isotropic shifts are governed by the magnitude of hyperfine coupling between the magnetic moments of the unpaired electronic spins and the nuclear magnetic moments of ^{6}Li or ^{7}Li nuclei, the accuracy of predictions depends predominantly on the accuracy of the determination of electronic spin density at the position of the above-mentioned nuclei. It was shown that very good predictions of hyperfine coupling constants and isotropic shifts could be obtained using DFT, pseudo-potentials, and the Projector Augmented-Wave (PAW) approach.[16,24]

In this work, we have used ^{57}Fe Mössbauer spectroscopy and ^{6}Li solid-state MAS NMR spectroscopy to investigate Li_2FeSiO_4 polymorphs. A systematic study on several samples prepared at different temperatures has been performed. The analysis of NMR spectra has been complemented by first-principles calculations of hyperfine coupling constants and elements of the *g*-tensor. The obtained results are correlated with the structural models determined in our recent publications.[7,8] The knowledge about the local structure of the Li_2FeSiO_4 polymorphs, and about the spectroscopic methods to investigate this structure, has been used for the characterization of a typical carbon-coated Li_2FeSiO_4 sample prepared at 700 °C and slowly cooled to room temperature.

EXPERIMENTAL SECTION

Different LFS polymorphs were prepared by annealing pristine hydrothermally prepared LFS samples in sealed stainless steel tubes filled with an argon atmosphere. Samples were heated for 6 h at selected temperatures (400, 700, and 900 °C) and quenched to 25 °C. The detailed synthesis procedure is described in ref 8. A typical sample for electrochemical characterization was prepared by mixing citric acid (1.3 g) and an as-prepared hydrothermal sample (1 g). It was heat-treated at 700 °C in a CO/CO_2 atmosphere for 6 h and slowly cooled to room temperature.

Powder X-ray diffraction (XRD) patterns of as-prepared LFS polymorphs were measured using Cu $K\alpha_{1,2}$ radiation at 298 K. The machine was equipped with a LinxEye detector that allows energy discrimination (to remove part of the fluorescence). The data were recorded in the 2θ range of 10°−90° with a 2θ step size of ∼0.02° and with a constant counting time of 12 s per step. The patterns were analyzed by full pattern matching and Rietveld refinements, as implemented in the Fullprof program.[25]

^{57}Fe Mossbauer experiments were performed in transmission geometry at 298 K. The source was ^{57}Co in a Rh matrix. Velocity calibration and isomer shifts (IS) were quoted relative to an absorber of metallic iron at room temperature. Parameter fits were performed using a standard least-squares fitting routine with Lorentzian lines.

Differential thermal analysis was performed over a range of 25−950 °C under a constant flow of argon, using a Simultaneous Thermal Analyzer STA 449 °C Jupiter (from Netzsch), and a heating/cooling rate of 10 °C min^{-1}.

Solid-state ^{6}Li magic-angle spinning (MAS) NMR spectra were recorded on a 600 MHz Varian NMR system, operating at a ^{6}Li Larmor frequency of 88.274 MHz, with a rotation-synchronized Hahn-echo pulse sequence. The sample rotation frequency was 20 kHz, the repetition delay between consecutive scans was 0.1 s, and the number of scans was 15 000. Frequency axis (in ppm) is reported relative to the lithium signal of a 1 M LiCl solution. Spinning-sideband powder patterns were analyzed using the Spinevolution simulation package[26] and "dmfit" software.[27] In addition to electron−nucleus dipolar interaction, electric quadrupolar interaction was also considered when fitting the spectra of ^{6}Li nuclei.

First-principles calculations were performed using the density functional theory (DFT) in the generalized gradient approximation of Perdew−Burke−Ernzerhof (GGA PBE)[28] with plane-wave basis and norm-conserving pseudo-potentials. In the first step, the atomic coordinates of atoms within LFS polymorphs were relaxed and optimized with Quantum Espresso's *pwscf* program.[29] The "final" ground state energies were then recalculated with the optimized geometries. In all calculations, the plane-wave cutoff energy was 1360 eV. The reciprocal-space sampling was performed with *k*-point grids of 4 × 4 × 4 points. All-electron information was reconstructed using the Projector Augmented-Wave (PAW)[16,24] and Gauge-Including Projector Augmented-Wave (GIPAW)[30,31] methods, as implemented in Quantum Espresso's GIPAW module.[29] The module yielded hyperfine coupling constants and elements of *g*-tensors, which were then used for quantitative prediction of the isotropic shifts.

RESULTS AND DISCUSSION

In our recent works,[7,8] we showed that at least three polymorphs of Li_2FeSiO_4 can be isolated through careful quenching procedures. A stoichiometric sample without impurities prepared by hydrothermal synthesis can serve as a good starting point for the isolation of different LFS polymorphs at different temperatures. Thermogravimetric data (Figure 1a) showed a small loss of mass in the temperature range up to 300 °C, related to the desorption of physically and chemically adsorbed water.[32] The

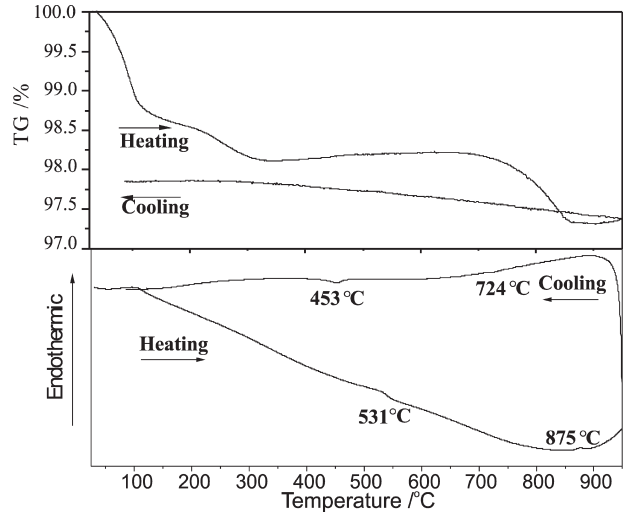

Figure 1. (a) TGA curve of pristine hydrothermal LFS sample and (b) corresponding normalized DSC data during heating and cooling processes at 10 °C/min under an argon atmosphere.

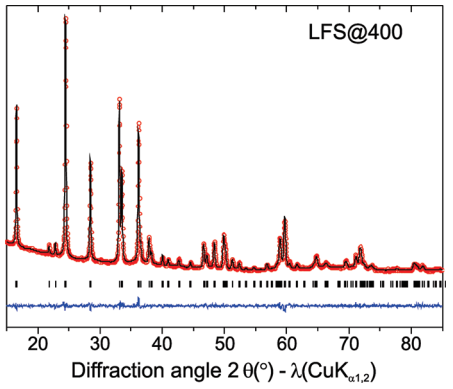

Figure 2. Rietveld refinement of the powder X-ray diffraction (XRD) pattern of LFS@400 ($Pmn2_1$ space group, a = 6.267(4) Å, b = 5.335 (2) Å, c = 4.965(3) Å).

reason for the additional loss of mass in the temperature range of 700−800 °C is not clear at the present stage. More important information is obtained from the DSC data (Figure 1b), where exothermic peaks during heating and endothermic peaks during cooling clearly delimit the stability ranges of the three polymorphs. The DSC diagram upon heating displays a steep curve, because of the agglomeration of small initial particles, which hinders the possibility of precise determination of the phase-transition enthalpies. The low-temperature polymorph β ($Pmn2_1$) transforms to the high-temperature polymorph γ_s ($P2_1/n$) at a temperature of ∼530 °C. The phase-transition temperature from the γ_s polymorph to the γ_{II} ($Pmnb$) polymorph was determined to be close to 875 °C upon heating. The phase transitions are reversible throughout the cooling process with the temperature of ∼724 °C for transition from the γ_{II} polymorph to the γ_s polymorph, and ∼453 °C for the transition from the γ_s polymorph to the β polymorph. Using the DSC data, we have isolated three different samples by quenching as-prepared hydrothermal samples sealed in stainless steel tubes filled with argon from 400 °C (LFS@400), 700 °C (LFS@700), and 900 °C (LFS@900) to 25 °C.

Table 1. Atomic Coordinates, Occupancies and Reliability Factors Obtained by Rietveld Refinement of XRD Data for LFS@400 (Space Group $Pmn2_1$)[a]

LFS@400					
site	Wyckoff	occupancy	x	y	z
Li1	4b	1	0.754(2)	0.334(3)	0.988(1)
Fe1	2a	1	0	0.1740(1)	0.450(2)
Si	2a	1	0	0.8260(3)	0.966(1)
O1	2a	1	0	0.8209(3)	0.314(4)
O2	2a	1	0	0.1147(4)	0.893(3)
O3	4b	1	0.789(0)	0.6795(1)	0.871(3)

[a] Lattice parameters: a = 6.2674(6) Å, b = 5.3352(7) Å, c = 4.9653(5) Å. R_f = 6.29%, V/z = 83.013. Twin mirror at Z = 0.956(1) with 0.68 multiplicity of predominant image.

Table 2. Selected Bond Lengths and Angles of the LFS@400 Sample

	O1	O2	O3	O3
		LiO_4		
O1	**1.992(2)**	105.7(4)	107.3(2)	110.8(3)
O2	3.176(3)	**1.991(2)**	108.6(2)	113.6(4)
O3	3.156(1)	3.181(2)	**1.925(0)**	110.3(2)
O3	3.238(3)	3.292(1)	3.173(3)	**1.941(2)**
		SiO_4		
O1	**1.731(1)**	104.09(3)	106.53(3)	106.53(3)
O2	2.614(1)	**1.582(1)**	114.02(5)	114.02(5)
O3	2.676(0)	2.674(3)	**1.606(3)**	110.80(4)
O3	2.676(0)	2.674(3)	2.644(5)	**1.606(3)**
		FeO_4		
O1	**2.000(2)**	101.47(4)	107.49(5)	107.49(5)
O2	3.273(2)	**2.223(2)**	104.3(2)	104.3(2)
O3	3.234(4)	3.346(4)	**2.011(0)**	128.49(3)
O3	3.234(4)	3.346(4)	3.622(3)	**2.011(0)**

All samples were checked via Rietveld refinement of powder XRD patterns. The refinements of LFS@700 and LFS@900 were based on the structural models that were recently reported in the literature[6−8] and are given in the Supporting Information. The structural model for LFS@400 was obtained using the coordinates of β-Li_3PO_4 and Li_2MnSiO_4.[3,33] The calculated versus experimental plots are given in Figure 2; the atomic coordinates, lattice parameters, and reliability factors are given in Table1, and the bond lengths and angles are given in Table2.

A close look at the local environments of Fe^{2+} in each polymorph reveals interesting differences. In all polymorphs, Fe^{2+} atoms are in tetrahedral coordination, surrounded by two LiO_4 tetrahedra, by one FeO_4 tetrahedron, and by one SiO_4 tetrahedron. The differences between iron environments are in the connectivity and in the orientations of the tetrahedra. In LFS@400 sample ($Pmn2_1$ space group), all tetrahedra share corners, and they are all pointing in the same direction along the c-axis (Figure 3a). The structures of the high-temperature polymorphs (LFS@700 and LFS@900) are more complicated. In the $P2_1/n$ (LFS@700) phase FeO_4 shares one edge with LiO_4 tetrahedron (Figure 3b), whereas in the $Pmnb$ one (LFS@900) FeO_4 shares

dx.doi.org/10.1021/cm103193a |Chem. Mater. 2011, 23, 2735–2744

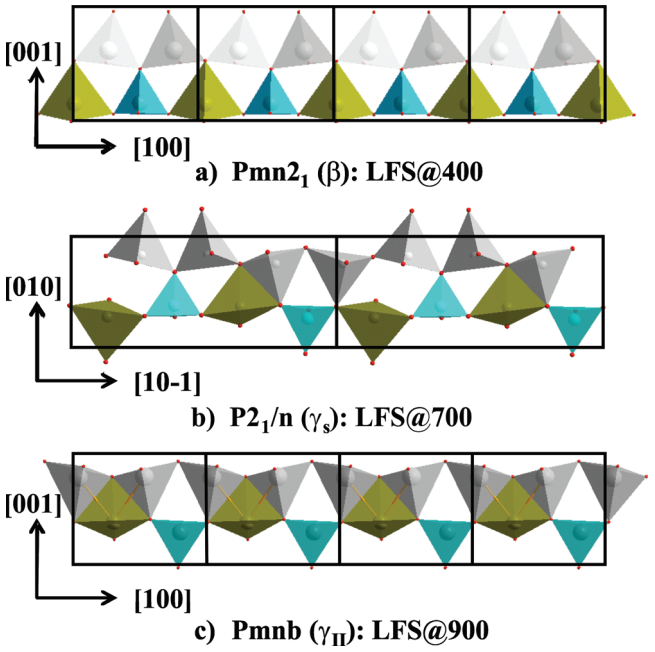

Figure 3. Comparisons between the tetrahedral orientations along equivalent directions in (a) LFS@400, (b) LFS@700, and (c) LFS@900.

two edges with LiO_4 tetrahedra (Figure 3c). The orientation of tetrahedra in the high-temperature polymorphs alternates in their pointing direction: up−up−down−down−up−up−down−down for the $P2_1/n$ structure (LFS@700) and up−down−up−down−up−down−up−down for the *Pmnb* structure (LFS@900). The alternation of Fe and Si (Fe−Si−Fe−Si-Fe) is common for all three structures. Differences in the tetrahedra connectivity and in the orientation have an influence on the average bond length in the FeO_4 tetrahedra. The general trend observed is a decrease of the average Fe−O bond length from 2.061(3) Å in LFS@400 to 2.026(1) Å in LFS@900 with intermediate value (2.032(1) Å) for LFS@700. Based on the crystallographic data, an opposite correlation was determined for the distortion of FeO_4 tetrahedra.[34] The largest distortion was found in the LFS@900 sample (12.8×10^{-4} Å^3) and the smallest in LFS@400 sample (2.3×10^{-4} Å^3), while the distortion in the LFS@700 sample was 9.9×10^{-4} Å^3.[35]

■ MÖSSBAUER SPECTROSCOPY

Those significant variations in the local environments of FeO_4 tetrahedra among all Li_2FeSiO_4 polymorphs can be addressed through Mössbauer spectroscopy, as previously reported for iron oxides and iron fluorides.[11] The Mössbauer spectra of the three polymorphs used in this work are gathered in Figure 4 and give a precious information on the quality of the samples investigated: only LFS@400 showed traceable amount of additional iron (below 2 at. %) in different local environments. In addition, the samples do not contain any detectable traces of Fe^{III}- or other Fe^{II}-containing oxides, contrary to what had been reported by Thomas et al.[2] The parameters (isomer shift and quadrupole splitting) of fitted spectra are within the ranges commonly observed for Fe in tetrahedral coordination[11] but are significantly different from one sample to another. Noticeably, each spectrum could be fitted nicely (χ^2 within a range of 3σ) with only one contribution from Fe, in full accordance with the crystal

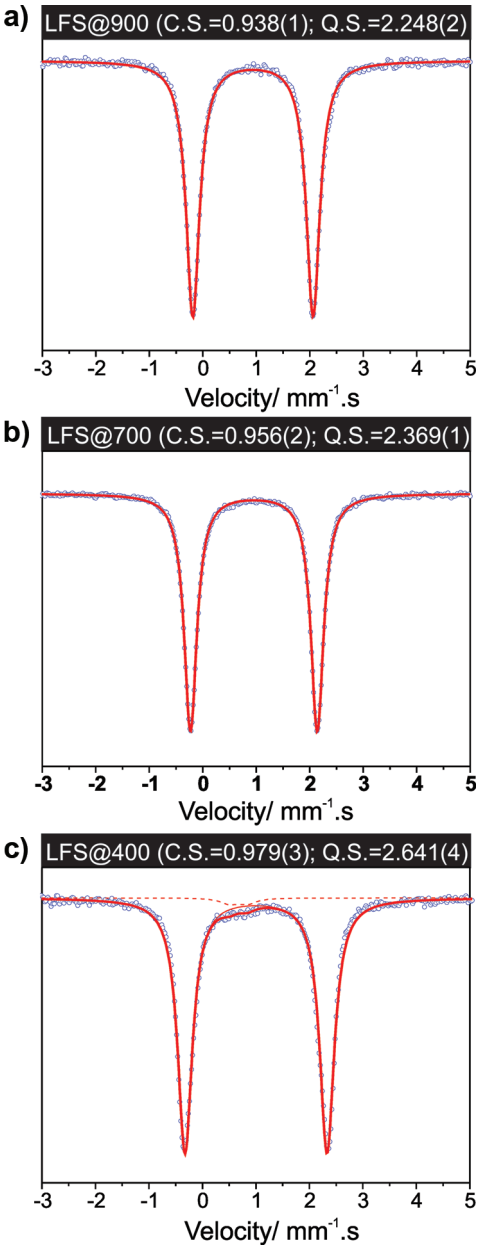

Figure 4. Mössbauer spectra for (a) LFS@900, (b) LFS@700, and (c) LFS@400 samples.

structures of the three polymorphs, each of them comprising only one Fe crystallographic site.

Interestingly, the respective chemical shifts of the three samples follow a general trend observed in other systems:[11] the increase in the covalent nature of the Fe−O bond (decrease in the average bond length) translates to a smaller chemical shift, from 0.94 mm s^{-1} (LFS@900) to 0.98 mm s^{-1} (LFS@400) (Figure 4). Those observations were validated for many samples and are reproducible (see Figure 5).

Even larger differences between samples were observed when comparing the quadrupole splitting values, which can be strongly correlated to the degree of the distortion of the FeO_4 tetrahedra, as reported by Dyar et al. for Fe in staurolite samples.[36] The trend of smaller quadrupole splitting for a higher distortion, observed here, cannot be taken as a general one in Mössbauer

spectroscopy but can be used in a particular system where Fe^{2+} have the same type and number of ligands.

^{6}Li MAS NMR

As in our recent work on Li_2MnSiO_4,[16] we measured the ^{6}Li MAS NMR spectra on different Li_2FeSiO_4 polymorphs in order to strengthen the information about the local structure, gathered so far through diffraction (electron, X-ray, neutron) and Mössbauer spectroscopy. The NMR spectra of LFS@400, LFS@900, and LFS@700 are shown in Figure 6. All three spectra exhibit broad spinning-sideband patterns that reflect the strong anisotropic dipolar interactions of lithium nuclei with electronic spins of paramagnetic centers, which are predominantly Fe ions (and, to a smaller extent, if electronic spins are partly delocalized, also O ions). Compared to lithium NMR signals of Li_2MnSiO_4 polymorphs, individual centerbands and sidebands in spectra of LFS polymorphs are ~10 times broader. While the full width at half maximum (fwhm) of the former was ~6−7 ppm, the fwhm of the latter is ~60−70 ppm. The difference in linewidths cannot be attributed to different relaxation rates, because ^{6}Li T_2 relaxation times of all Li_2MnSiO_4 and Li_2FeSiO_4 polymorphs are almost the same; they are ~3 ms long and correspond to linewidths of ~1 ppm. Therefore, the much-stronger broadening of the centerbands and sidebands in the spectra of Li_2FeSiO_4 must be produced via another mechanism, most probably by the anisotropic bulk magnetic susceptibility effect, as discussed later in the text.

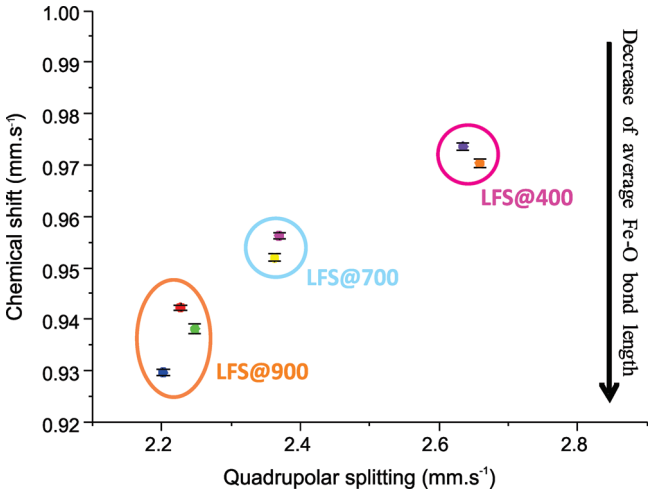

Figure 5. Relationships between quadrupole splitting (QS) and chemical shift (IS) for LFS polymorphs prepared at different temperatures (only samples without detectable impurities were used in this study).

LFS@400 and LFS@900 samples both exhibit a single lithium contribution with isotropic positions of −72 and −30 ppm, respectively. This is consistent with the proposed crystal structures for $Pmn2_1$ (LFS@400) and *Pmnb* (LFS@900) polymorphs, which both contain a single lithium site within their asymmetric crystallographic units. On the other hand, the spectrum of LFS@700 can be decomposed into two equally strong contributions (intensity ratio of 0.49:0.51). The isotropic positions of the two contributions are −7 and −55 ppm, as previously mentioned by Quoirin.[37] Because of large linewidths, the two contributions severely overlap, yielding slightly asymmetric NMR centerband and sidebands. Perhaps easier to rationalize than the difference in isotropic positions of the two lithium contributions is the difference in widths of their spinning-sideband patterns (see Figure 7). As already mentioned, the width of the sideband pattern depends on the magnitude of the dipolar interaction of lithium nuclei with paramagnetic centers, which, in turn, depends on the distances between the nuclei and the centers. Inspecting the proposed structure of $P2_1/n$ polymorph,[38] one can distinguish two equally populated lithium sites. While the $Li(2)O_4$ tetrahedron shares corners with four neighboring

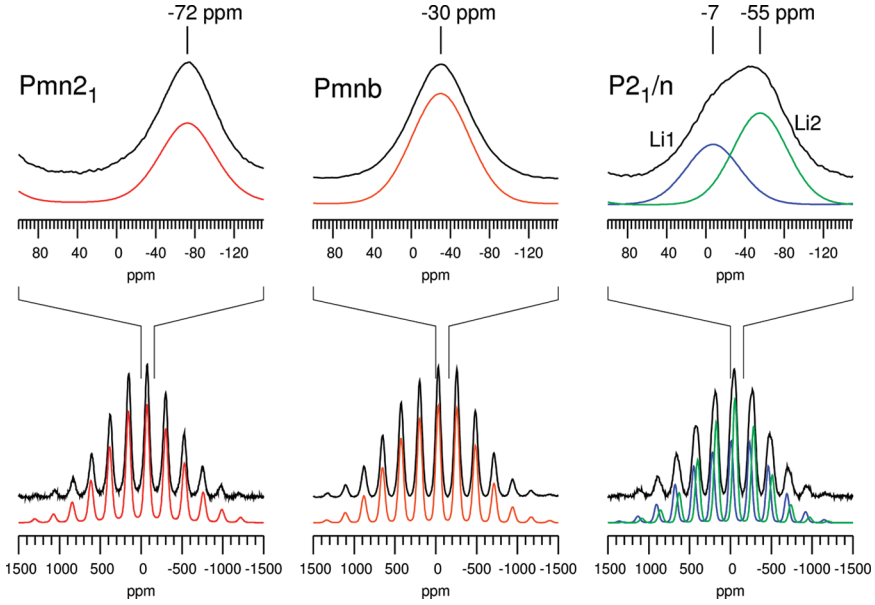

Figure 6. ^{6}Li MAS NMR spectra of $Pmn2_1$ (LFS@400 sample), *Pmnb* (LFS@900 sample), and $P2_1/n$ polymorphs (LFS@700 sample). The bottom part of the figure shows entire spectra with broad spinning-sideband patterns. The top part of the figure shows isotropic bands (centerbands) of the three spectra. Spectra of LFS@400 and LFS@900 can be well-fitted by a single Li contribution. The spectrum of LFS@700 can be described as a sum of two contributions; one is plotted in green, another in blue. Solid black lines represent measured spectra.

dx.doi.org/10.1021/cm103193a |*Chem. Mater.* 2011, 23, 2735–2744

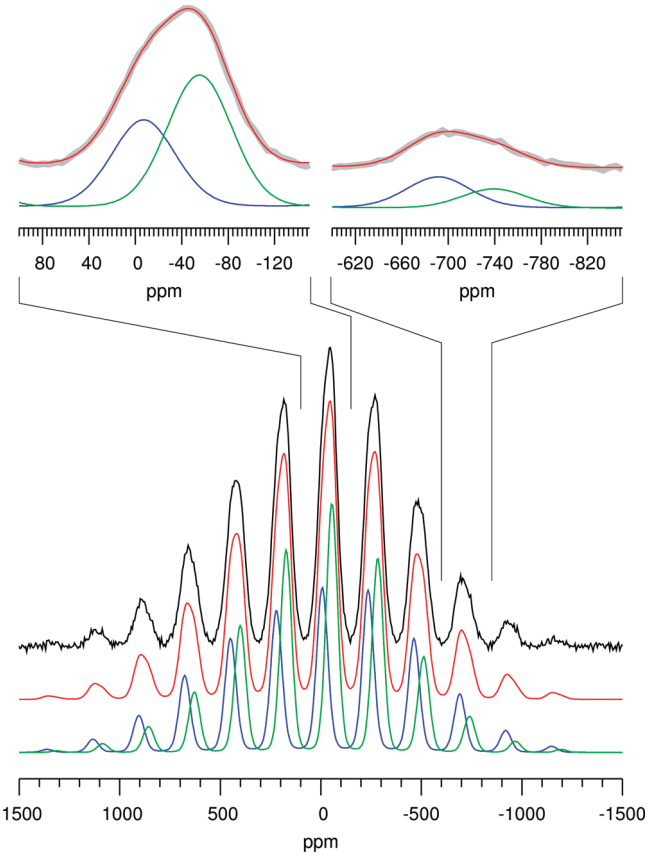

Figure 7. The decomposition of the ^{6}Li MAS NMR spectrum of the $P2_1/n$ polymorph (LFS@700) into two contributions. Although the centerbands and the sidebands of the two contributions overlap severely, they produce asymmetric peaks, which still allow relatively reliable decomposition (especially because the spinning-sideband patterns of the two contributions are differently broad and, thus, the "asymmetric shape of the peaks" changes with the rank of the sideband).

FeO_4 tetrahedra, the Li(1)O_4 tetrahedron shares corners with two and an edge with one of the neighboring FeO_4 tetrahedra (see Figure 3). The distances between Li and Fe sites in edge-sharing tetrahedra are substantially shorter than the distances between lithium and iron sites in corner-sharing tetrahedra. The first amounts to ~0.28 nm and the second exceeds 0.3 nm. Because of the short distance, the interaction between Li(1) nuclei and iron centers is stronger, and the induced width of the NMR spinning-sideband powder pattern is larger. Tentatively, a narrower powder pattern with isotropic shift of −55 ppm can be assigned to the Li(2) site, and a broader powder pattern with isotropic shift of −7 ppm can be assigned to the Li(1) site.

The width and the shape of the spinning-sideband powder patterns can be assessed also more quantitatively. Nayeem and Yesinowski[39] showed that the effect of through-space dipolar interaction between the nuclear spin and several paramagnetic centers can be described by the Hamiltonian

$$H_{en} = \hbar\gamma \mathbf{B}_0 \sigma_{en} \mathbf{I} \qquad (1)$$

where γ is the nuclear gyromagnetic ratio, $\mathbf{B}_0$ the external magnetic field, and $\mathbf{I}$ the nuclear spin operator. The tensor

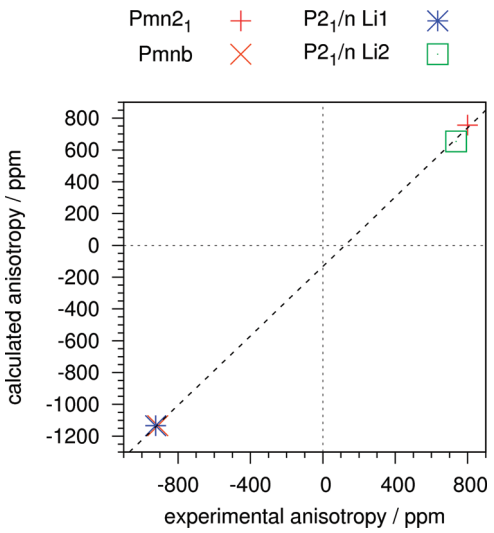

Figure 8. Calculation of tensors, describing through-space electron−nucleus dipolar interaction. The graph shows the correlation between the measured and the calculated dipolar-interaction anisotropy parameters for four Li sites in LFS polymorphs.

$\boldsymbol{\sigma}_{en}$ can be expressed as

$$\sigma_{en} = \frac{\mu_0}{4\pi}\left[\frac{\mu_B{}^2 S(S+1)}{3kT}\right]\mathbf{g}\cdot\mathbf{g}\cdot\mathbf{D}_{en} \qquad (2)$$

where μ_B is the Bohr magneton, S the spin of the paramagnetic center, and $\mathbf{D}_{en}$ the dipolar matrix ($D_{\alpha\beta} = \Sigma_i(\delta_{\alpha\beta} - 3e^i_\alpha e^i_\beta)/r_i{}^3$), which contains only information about the positions of paramagnetic centers with respect to the nucleus. Other symbols have their usual meaning.

If we assume the **g**-tensor to be isotropic and equal to 2, we can verify if meaningful prediction of the spinning-sideband powder patterns of ^{6}Li MAS NMR spectra can be obtained solely based on the geometrical information about the arrangement of Fe^{2+} ions around Li nuclei. We calculated the $\boldsymbol{\sigma}_{en}$ tensors for the Li sites of the $P2_1/n$, $Pmn2_1$, and $Pmnb$ polymorphs, using the proposed structures and assuming that spin-delocalization is negligible. We took into account all the Fe sites within a sphere with a radius of 0.8 nm around a selected Li nucleus and estimated the effective magnetic moment using a theoretical Bohr magneton number for Fe^{2+} ions of 4.9,[40] anticipating that the crystal field was much stronger than the spin−orbit coupling. The calculated anisotropy parameters σ^{aniso}_{en} are compared to the experimentally obtained values in Figure 8. The latter anisotropy parameters were actually extracted from ^{6}Li MAS NMR spectra by using the simulations of spinning-sideband patterns (see the Supporting Information). In addition to the interaction with paramagnetic centers, the sideband patterns of ^{6}Li MAS NMR spectra are affected also by electric quadrupolar interaction.[41] Chemical shift anisotropy and nuclear dipole−dipole couplings are negligible and were not taken into account in the analysis of the sideband patterns. We also did not take into account the bulk magnetic susceptibility (BMS) effect. In diamagnetic materials, broadening due to BMS is usually rather small and is spun away by magic-angle spinning (MAS).[42,43] In paramagnetic materials, however, the BMS effect can be large and often cannot be entirely removed by MAS. In some cases, it can contribute substantially to sideband intensities.[41] Quantitatively, the BMS contribution

dx.doi.org/10.1021/cm103193a |*Chem. Mater.* 2011, 23, 2735–2744

Table 3. NMR Parameters[a] Obtained Via the Analysis of ^{6}Li MAS NMR Spectra

	δ^{iso} [ppm]	σ_{en}^{aniso} [ppm]	η_{en}	χ_Q [kHz]	η_Q
LFS@400	−72	800	1.0	24	1.0
LFS@900	−30	−910	1.0	22	0.3
LFS@700 Li1	−7	−920	1.0	21	0.2
LFS@700 Li2	−55	740	1.0	24	1.0

[a] $\sigma_{en}^{iso} = \mathrm{Tr}\{\boldsymbol{\sigma}_{en}\}/3$, $\sigma_{en}^{aniso} = \sigma_{en}^{ZZ} - \sigma_{en}^{iso}$, $\eta_{en} = (\sigma_{en}^{YY} - \sigma_{en}^{XX})/\sigma_{en}^{aniso}$, $|\sigma_{en}^{ZZ} - \sigma_{en}^{iso}| \geq |\sigma_{en}^{XX} - \sigma_{en}^{iso}| \geq |\sigma_{en}^{YY} - \sigma_{en}^{iso}|$, $\chi_Q = e^2Qq/h$, $\eta_Q = (V^{YY} - V^{XX})/V^{ZZ}$, $|V^{ZZ}| \geq |V^{XX}| \geq |V^{YY}|$. σ_{en}^{XX}, σ_{en}^{YY}, and σ_{en}^{ZZ} are diagonal components of the $\boldsymbol{\sigma}_{en}$ tensor in its principal axes system. V^{XX}, V^{YY}, and V^{ZZ} are diagonal components of the electric field gradient tensor **V** in its principal axes system.

to spinning-sideband pattern is, unfortunately, very difficult to assess, and its analysis exceeds the scope of this paper.

The results of the analysis of sidebands patterns, taking into account only electron−nucleus dipolar and electric quadrupolar interactions, are collected in Table 3. The above-mentioned approximations, especially the neglected BMS effect, might be responsible for the slight disagreement between the measured and the simulated NMR spectra (see the Supporting Information). Because of that, the anisotropy parameters extracted by the analysis of spinning-sideband intensities can be considered more as estimates than as precisely measured values. Nevertheless, they still correlate well with the predicted anisotropy parameters and can be rationalized by the differences in the symmetry of the local Li environments. The Li site of $Pmn2_1$ and Li(2) site of $P2_1/n$ polymorphs are surrounded by four Fe^{2+} ions that are sitting in the corners of slightly distorted tetrahedra. Such relatively symmetric environments lead to quite small electron−nucleus anisotropy parameters. The Li(1) site of the $P2_1/n$ polymorph and the Li site within the *Pmnb* polymorph are both bonded to only three Fe^{2+} ions and occupy less-symmetric positions slightly above triangles of Fe^{2+} ions. Li on these sites experiences larger anisotropy of electron−nucleus dipolar interaction. Very similar differences in σ_{en}^{aniso} were observed already for Li nuclei surrounded by either four or three Mn^{2+} ions within the Li_2MnSiO_4 polymorphs.[16] The magnitudes of the anisotropy parameters in LFS and LMS materials are also comparable, suggesting that the BMS effect does not dominate the spinning-sideband patterns. Most likely, it affects only intensities of the lowest-rank sidebands (zeroth, first, second), which is probably why the fitting/simulation process in all Li_2FeSiO_4 polymorphs converged to an asymmetry parameter value of $\eta_{en} = 1$.

As in the case of Li_2MnSiO_4, the anisotropy parameters thus again reflect the short-range structural motifs of the polymorphs and enable the assignment of two detected NMR contributions to two Li sites of the $P2_1/n$ polymorph. However, the anisotropy parameters of the Li site of the *Pmnb* polymorph and the Li(1) site of the $P2_1/n$ polymorph hardly differ from each other. This means that, based only on σ_{en}^{aniso}, we cannot distinguish between the two Li environments. In contrast, although the centerbands are relatively broad, we can still distinguish different isotropic shifts for the four different Li sites within the three polymorphs. In the case of the Li_2MnSiO_4 polymorphs, the isotropic shifts were determined by the strength of hyperfine coupling of lithium nuclei with unpaired elecronic spins. The hyperfine coupling constants were successfully predicted by the DFT Projector-Augmented-Wave (PAW) approach,[16] and

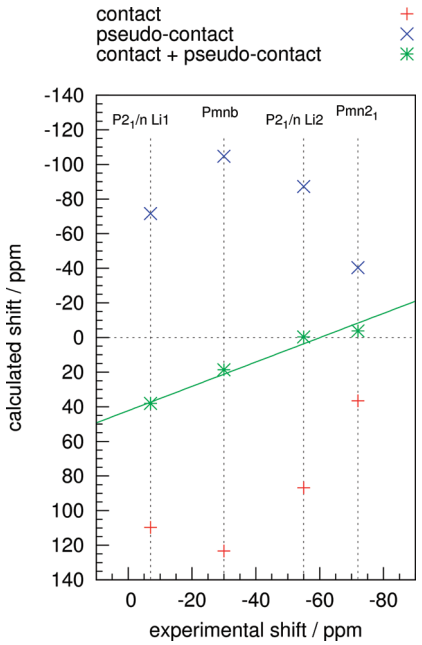

Figure 9. Correlation between the measured and the calculated (using DFT with either PAW or GIPAW reconstruction) contact, pseudo-contact, and total isotropic shifts due to electron−nucleus hyperfine and dipolar interactions in LFS polymorphs.

the isotropic shifts obtained from them agreed well with the measured values.

Along the same lines as those for the Li_2MnSiO_4 polymorphs, we tried to reproduce the measured isotropic shifts by theoretical calculations also for Li_2FeSiO_4. However, with the available norm-conserving pseudo-potentials and within the implemented generalized gradient approximation of Perdew−Burke−Ernzerhof (GGA PBE), the calculated *contact (hyperfine)* isotropic shifts for all four different Li sites were small and positive. In addition to potential limitations in the accuracy of the first-principles calculations, the discrepancy between the measured and the calculated isotropic shifts in iron-containing paramagnetic materials also could stem from the so-called "*pseudo-contact*" shift. Such a shift can be expected when the magnetic susceptibility of a material is anisotropic. Because the anisotropy of the magnetic susceptibility or the anisotropy of the **g**-tensor could not be measured in the powdered LFS polymorphs, we again used the GIPAW module of the Quantum Espresso code[29] to predict the anisotropy of the **g**-tensor from first principles[31] (based on known crystal structures). When the **g**-tensor was obtained, it was inserted into eq 2, and the isotropic pseudo-contact shift was then simply calculated as

$$\delta^{PC} = \frac{1}{3} Tr\{\sigma_{en}\} \qquad (3)$$

Afterward, the total isotropic shift was obtained as a sum of two contributions: a contact shift and a pseudo-contact shift.

The results of calculations are presented in Figure 9. In all cases, the pure pseudo-contact shift for lithium nuclei was negative. The magnitude of the pseudo-contact shift was comparable to the magnitude of the contact shift. Although the sum of two contributions in only one case led to a negative total isotropic shift, and in three cases led to slightly positive isotropic shifts, the correlation with the measured values is still fine. More

dx.doi.org/10.1021/cm103193a |*Chem. Mater.* 2011, 23, 2735–2744

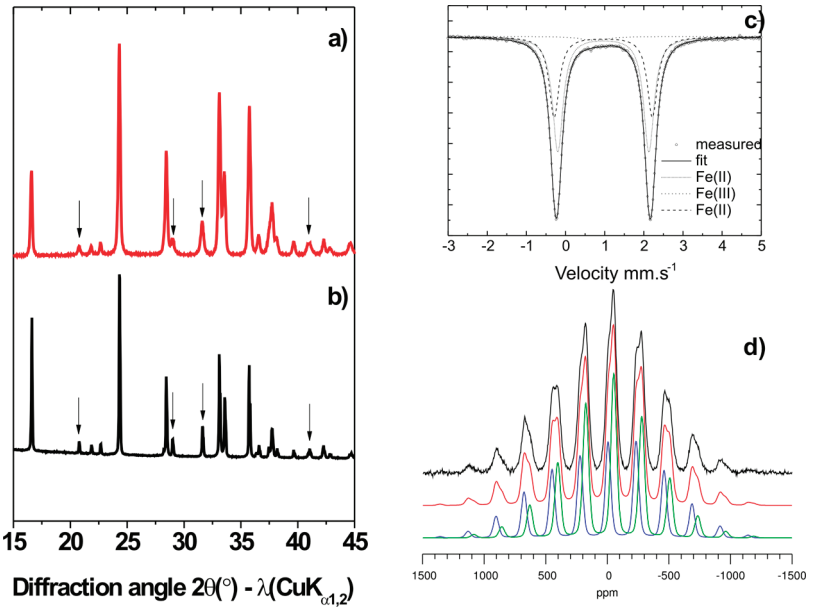

Figure 10. (a) Powder XRD pattern, (b) simulated XRD pattern (space group $P2_1/n$), (c) ^{57}Fe Mössbauer spectrum, and (d) ^{6}Li MAS NMR spectrum of the battery sample.

importantly, these calculations prove that, in the case of LFS materials, pseudo-contact shifts induced by the anisotropy of the **g**-tensor are not negligible and substantially contribute to the total isotropic shift. The calculations also show that rough quantitative estimations of pseudo-contact shifts are possible. To the best of our knowledge, this is the first quantitative analysis of pseudo-contact paramagnetic shifts in lithium-based materials.

Quite expectedly, analogous calculations on Li_2MnSiO_4 polymorphs show that the **g**-tensor anisotropy is negligible in these materials. Since the **g**-tensor anisotropy is directly related to the anisotropy of magnetic susceptibility, it seems reasonable that extensive broadening of centerbands and sidebands observed in ^{6}Li NMR spectra of Li_2FeSiO_4, but not in the spectra of the Li_2MnSiO_4, is produced by this broadening mechanism. Note the difference between the previously discussed BMS effect and the just-mentioned anisotropic bulk magnetic susceptibility (ABMS) effect. The former (BMS) is larger and is important, even when the magnetic susceptibility tensor is isotropic. It does not affect the width of the centerbands and the sidebands, but, if strong enough, it can affect the intensities of the sidebands (i.e., it can affect the spinning-sideband pattern). The latter (ABMS) mechanism is effective only when the magnetic susceptibility tensor is anisotropic. In that case, the ABMS tensors of randomly oriented crystallites around a given crystallite generate a local magnetic field ,which varies from crystallite to crystallite in the sample. This means that ^{6}Li nuclei in different parts of the sample resonate at slightly different frequencies, leading to inhomogeneous line broadening of centerbands and sidebands.

We can roughly estimate the contribution of the ABMS to the width of the NMR signals. VanderHart[42] showed that, for an axially symmetric ABMS under MAS, the NMR frequencies are spread between $2\pi(\chi_{||} - \chi_{\perp})/3$ and $-\pi(\chi_{||} - \chi_{\perp})/3$. Here, χ and $\chi_{\perp}$ are the parallel and perpendicular components of the volume magnetic susceptibility tensor, respectively. For the LFS@900 sample, for which the calculated **g**-tensor is almost axially symmetric, the calculated difference $\pi(\chi_{||} - \chi_{\perp})/3$ is equal to 37 ppm. This confirms that linewidths of 60−70 ppm, as detected in LFS samples, indeed stem from ABMS broadening. Unfortunately, linewidths of the ^{6}Li MAS NMR signals cannot be assessed entirely quantitatively. The extent of the ABMS broadening, namely, does not depend only on the difference $\chi_{||} - \chi_{\perp}$, but also on the shape, size, and the packing of the crystallites.

CARBON-COATED Li_2FeSiO_4 SAMPLE

As an example of the application of the above-described spectroscopic techniques for the analysis of more-demanding materials, a carbon-coated Li_2FeSiO_4 sample ready for the electrochemical characterization was studied. The sample was prepared by heat treatment at 700 °C, followed by slow cooling to room temperature. Basically, it can be described as a LFS@700 sample, because its XRD pattern (Figure 10a) is very similar to the pattern of the Li_2FeSiO_4 crystallized in the $P2_1/n$ space group (simulated pattern is shown in Figure 10b). Hardly observable differences between patterns are observed, only in the width (fwhm) of the diffraction peaks typical for the LFS@700 phase (see arrows in Figures 10a and 10b). These "imperfections" in the XRD pattern are much more pronounced in the Mössbauer spectrum (Figure 10c). The fit of the spectrum shows that some of the iron (58 at. %) has a similar environment as the iron in the LFS@700 sample, whereas another major portion of iron (40 at. %) exhibits a QS parameter close to that of the LFS@400 phase and the IS parameter is still similar to that of the LFS@700 sample. This indicates that phase transformation from the $P2_1/n$ polymorph to the $Pmn2_1$ polymorph started but had not yet been completed. A similar conclusion can be drawn from the NMR spectrum of the carbon-coated sample (Figure 10d). The spectrum can be described as a sum of two contributions with very similar environments to those of the pure LFS@700 phase. However, the ratio of populations of the two Li sites now deviates from 1:1 and amounts to 0.8:1 (Figure 10d). This suggests that the local environment of a substantial part of the lithium started to change.

dx.doi.org/10.1021/cm103193a |*Chem. Mater.* 2011, 23, 2735–2744

CONCLUSIONS

We showed that ^{57}Fe Mössbauer and ^{6}Li MAS NMR spectra were very sensitive to the local environment of cations in Li_2FeSiO_4, and that the parameters obtained from these spectra were giving typical values for each of the crystallographically pure Li_2FeSiO_4 polymorphs.

The polymorphs differ in the connectivity and in the orientation of the tetrahedra, which, together, affected the average Fe−O bond lengths, the distortion of the FeO_4 tetrahedra, and the connectivity scheme between LiO_4 and FeO_4 tetrahedra. Consequently, shorter Fe−O bonds (stronger covalent nature) give rise to smaller chemical shifts in the Mössbauer spectra. Average Fe−O bond lengths decrease as the temperature used for the isolation of a particular polymorph increases (i.e., the shortest bonds were detected in LFS@900 sample). The asymmetry parameter of the electron−nucleus dipole−dipole interaction, which could be obtained via an analysis of spinning-sideband patterns of ^{6}Li MAS NMR spectra, depended on the arrangement of Fe^{2+} ions around ^{6}Li nuclei. By inspecting the sideband pattern, we could easily discriminate between Li NMR signals that belong to those LiO_4 tetrahedra that only share corners with neighboring FeO_4 tetrahedra, and those LiO_4 tetrahedra that also share an edge with one of the neighboring FeO_4 tetrahedra. Analysis of ^{6}Li NMR isotropic shifts was the most demanding. The magnitude and the sign of the shift could not be plainly related to the geometrical description of the lithium local environment; the relationship between the structure and the isotropic shift was established only by using quantum-mechanical calculations. In the present case of Li_2FeSiO_4 polymorphs, the isotropic shifts were composed of the contact and the pseudo-contact shift. Based on known structures, both of them were estimated by DFT-based first principles calculations. The calculation of the pseudo-contact shift required knowledge of the components of the **g**-tensor, which were calculated ab initio, using the DFT/GIPAW approach. In Li_2FeSiO_4 polymorphs, the pseudo-contact shifts were of comparable amplitude but opposite sign as the contact shifts. The anisotropy of the **g**-tensor also was responsible for severe broadening of the NMR signals, which cannot be removed by magic-angle spinning (MAS). This broadening and the substantial pseudo-contact shift make the analysis of ^{6}Li MAS NMR spectra of Li_2FeSiO_4 polymorphs much more demanding than the analysis of NMR spectra of Li_2MnSiO_4 polymorphs. Spectroscopic investigation of pure Li_2FeSiO_4 polymorphs, and the knowledge gathered in this way, simplified the analysis of carbon-coated Li_2FeSiO_4 sample (i.e., it enabled easy identification of deviation from the pure structure).

ASSOCIATED CONTENT

Supporting Information. This material is available free of charge via the Internet at http://pubs.acs.org.

AUTHOR INFORMATION

Corresponding Author

*Tel.: +38614760362. Fax: +38614760422. E-mail: robert.dominko@ki.si.

ACKNOWLEDGMENT

The financial support from the Ministry of Education, Science and Sport of Slovenia, the Slovenian Research Agency, EN-FIST Centre of Excellence, and CO-NOT Centre of Excellence and the support from the ALISTORE European Research Institute (ERI) are acknowledged. The Ministère de l'Enseignement Supérieur et de la Recherche, France, is acknowledged for supporting CS through an International PhD Student Scholarship shared between Amiens (France) and Ljubljana (Slovenia). Matthieu Courty (LRCS) is thankfully acknowledged for performing the TG/DSC measurements.

REFERENCES

(1) Padhi, A. K.; Nanjundaswamy, K. S.; Goodenough, J. B. *J. Electrochem. Soc.* **1997**, *144*, 1188.
(2) Nyten, A.; Abouimrane, A.; Armand, M.; Gustafsson, T.; Thomas, J. O. *Electrochem. Commun.* **2005**, *7*, 156.
(3) Dominko, R.; Bele, M.; Gaberscek, M.; Meden, A.; Remskar, M.; Jamnik *J. Electrochem. Commun.* **2006**, *8*, 217.
(4) Nadherna, M.; Dominko, R.; Hanzel, D.; Reiter, J.; Gaberscek, M. *J. Electrochem. Soc.* **2009**, *156*, A619.
(5) Fan, X.-Y.; Li, Y.; Wang, J.-J.; Gou, L.; Zhao, P.; Li, D.-L.; Huang, L.; Sun, S.-G. *J. Alloy Compd.* **2010**, *493*, 77.
(6) Nishimura, S.; Hayase, S.; Kanno, R.; Yashima, M.; Nakayama, N.; Yamada, A. *J. Am. Chem. Soc.* **2008**, *130*, 13212.
(7) Boulineau, A.; Sirisopanaporn, C.; Dominko, R.; Armstrong, A. R.; Bruce, P. G.; Masquelier, C. *Dalton Trans.* **2010**, *39*, 6310.
(8) Sirisopanaporn, C.; Boulineau, A.; Armstrong, A. R.; Bruce, P. G.; Hanzel, D.; Budic, B.; Dominko, R.; Masquelier, C. *Inorg. Chem.* **2010**, *49*, 7446.
(9) Keffer, C.; Mighell, A. D.; Mauer, F.; Swanson, H.; Block, S. *Inorg. Chem.* **1967**, *6*, 119.
(10) Zemann, J. *Acta Crystallogr.* **1960**, *13*, 863.
(11) Menil, F. *J. Phys. Chem. Solids* **1985**, *46*, 763.
(12) Grey, C. P.; Dupre, N. *Chem. Rev.* **2004**, *104*, 4493.
(13) Lee, Y. J.; Grey, C. P. *Chem. Mater.* **2000**, *12*, 3871.
(14) Cabana, J.; Shirakawa, J.; Chen, G.; Richardson, T. J.; Grey, C. P. *Chem. Mater.* **2010**, *22*, 1249.
(15) Armstrong, A. R.; Lyness, C.; Menetrier, M.; Bruce, P. G. *Chem. Mater.* **2010**, *22*, 1892.
(16) Mali, G.; Meden, A.; Dominko, R. *Chem. Commun.* **2010**, *46*, 3306.
(17) Arroyo-deDompablo, M. E.; Dominko, R.; Gallardo-Amores, J. M.; Dupont, L.; Mali, G.; Ehrenberg, H.; Jamnik, J.; Moran, E. *Chem. Mater.* **2008**, *20*, 5574.
(18) Kunganathan, N.; Islam, M. S. *Chem. Mater.* **2009**, *21*, 5196.
(19) Frayret, C.; Masquelier, C.; Villesuzanne, A.; Morcrette, M.; Tarascon, J. M. *Chem. Mater.* **2009**, *21*, 1861.
(20) Kokalj, A.; Dominko, R.; Gaberscek, M.; Bele, M.; Mali, G.; Remskar, M.; Jamnik, J. *Chem. Mater.* **2007**, *19*, 3633.
(21) Carlier, D.; Menetrier, M.; Grey, C. P.; Delmas, C.; Ceder, G. *Phys. Rev. B* **2003**, *67*, 174103.
(22) Chazel, C.; Menetrier, M.; Carlier, D.; Croguennec, L.; Delmas, C. *Chem. Mater.* **2007**, *19*, 4166.
(23) Carlier, D.; Menetrier, M.; Delmas, C. *J. Phys. Chem. C* **2010**, *114*, 4749.
(24) Blöchl, P. E. *Phys. Rev. B* **1994**, *50*, 17953.
(25) Carvajal, J. R. *An introduction to the program FullProf 2000*; available at http://www.ill.eu/sites/fullprof/php/tutorials.html.
(26) Veshtort, M.; Griffin, R. G. *J. Magn. Reson.* **2006**, *178*, 248.
(27) Massiot, D.; Fayon, F.; Capron, M.; King, I.; Le Calve, S.; Alonso, B.; Durand, J. O.; Bujoli, B.; Gan, Z. H.; Hoatson, G. *Magn. Reson. Chem.* **2002**, *40*, 70.
(28) Perdew, J. P.; Burke, K.; Ernzerhof, M. *Phys. Rev. Lett.* **1999**, *77*, 3865.
(29) Giannozzi, P.; Baroni, S.; Bonini, N.; Calandra, M.; Car, R.; Cavazzoni, C.; Ceresoli, D.; Chiarotti, G. L.; Cococcioni, M.; Dabo, I.; Dal Corso, A.; de Gironcoli, S.; Fabris, S.; Fratesi, G.; Gebauer, R.; Gerstmann, U.; Gougoussis, C.; Kokalj, A.; Lazzeri, M.; Martin-Samos,

L.; Marzari, N.; Mauri, F.; Mazzarello, R.; Paolini, S.; Pasquarello, A.; Paulatto, L.; Sbraccia, C.; Scandolo, S.; Sclauzero, G.; Seitsonen, A. P.; Smogunov, A.; Umari, P.; Wentzcovitch, R. M. *J. Phys.: Condens. Matter* **2009**, *21*, 395502. (Also available via the Internet at http://www.quantum-espresso.org.)

(30) Pickard, C. J.; Mauri, F. *Phys. Rev. B* **2001**, *63*, 245101.

(31) Pickard, C. J.; Mauri, F. *Phys. Rev. Lett.* **2002**, *88*, 086403.

(32) Dominko, R. *J. Power Sources* **2008**, *184*, 462.

(33) Keffer, C.; Mighell, A. D.; Mauer, F.; Swanson, H.; Block, S. *Inorg. Chem.* **1967**, *6*, 119.

(34) Rodriguez-Carvajal, J. *Phys. Rev. Lett.* **1998**, *21*, 4660.

(35) Sirisopanaporn, C.; Masquelier, C.; Armstrong, R. A.; Bruce, P. G.; Dominko, R. *J. Am. Chem. Soc.* **2011**, *133*, 1263.

(36) Dyar, M. D.; Perry, C. L.; Rebbert, C. R.; Dutrow, B. L.; Holdaway, M. J.; Lang, H. M. *Am. Mineral.* **1991**, *76*, 27.

(37) Quoirin, G. Ph.D. Thesis, Université de Picardie Jules Verne, Amiens, France, 2007.

(38) Yamada, A.; Oral communication during the LiBD (Lithium Battery Discussion) Meeting held in Arcachon (France) in September 2009.

(39) Nayeem, A.; Yesinowski, J. P. *J. Chem. Phys.* **1988**, *89*, 4600.

(40) Ashcroft, N. W.; Mermin, N. D.; *Solid State Physics*; Saunders College Publishing: Fort Worth, TX, 1976.

(41) Lee, Y. J.; Grey, C. P. *J. Phys. Chem. B* **2002**, *106*, 3576.

(42) VanderHart, D. L.; Earl, W. L.; Garroway, A. N. *J. Magn. Reson.* **1981**, *44*, 361.

(43) Kubo, A.; Spaniol, T. P.; Terao, T. *J. Magn. Reson.* **1998**, *133* 330.